Reliable Hybrid Mixture Model for Generalized Point Set Registration

Zhengyan Zhang[1†], Zhe Min[2†], Ang Zhang[3], Jiaole Wang[1*], Shuang Song[1*], Max Q.-H. Meng[4], *Fellow, IEEE*

***Abstract*—Point set registration (PSR) is an essential problem in the field of surgical navigation and augmented reality. In surgical navigation, the aim of registration is mapping the pre-operative space to the intra-operative space. This paper introduces a reliable hybrid mixture model, in which the reliability of the normal vectors in the generalized point set (GPS) is examined and exploited. The motivation of considering the reliability of orientation information is that normal vectors cannot be estimated or measured accurately in the clinic. The point set is divided into two subsets according to the reliability of normal vectors. PSR is cast into the maximum likelihood estimation (MLE) problem. The expectation maximization (EM) framework is used to solve the MLE problem. In the E-step, the posterior probabilities between points in two point sets are computed. In the M-step, the transformation matrix and model components are updated by optimizing the objective function. We have demonstrated through extensive experiments on the human femur bone point set that the proposed algorithm outperforms the state-of-the-art ones in terms of accuracy, robustness, and convergence speed.**

***Index Terms*—Point set registration (PSR), surgical navigation, partial hybrid mixture model, maximum likelihood estimation (MLE), expectation maximization (EM).**

I. Introduction

POINT set registration (PSR) aims to estimate the transformation matrix between two sets of points [1]. It is an essential task in computer vision [2]–[4], robotics [5]–[7], computer-assisted surgery (CAS) [8], [9], medical image analysis [10], [11] and augmented reality (AR) surgical navigation system [12]–[14]. In CAS, PSR can be used to match the pre-operative space to the intra-operative space [15]. In the field of AR-assisted surgical navigation systems, PSR is usually used to align and overlay the virtual models to the physical space [13]. For example, in AR-guided total hip replacement surgery, the intra-operative point set (PS) of a femur bone is registered to the pre-operative three-dimensional model reconstructed by computer tomography (CT) or magnetic resonance imaging (MRI).

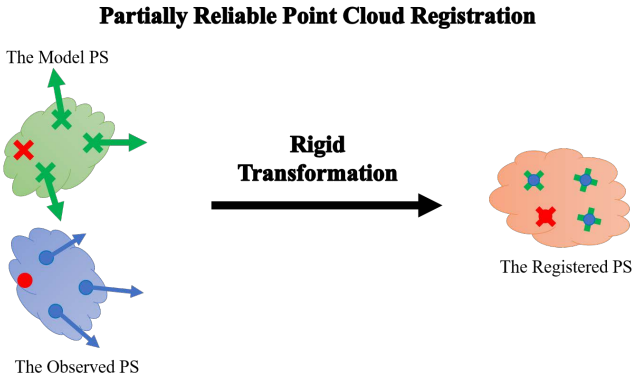

Fig. 1: Illustration of the proposed PSR algorithm. The reliability of normal vectors is incorporated into registration. The point with unreliable normal vector is represented as red dot both in the model PS and the observed PS. The points reliable normal vectors are denoted with green cross marks in the model PS and blue dots in the observed PS, respectively.

Optimization-based registration algorithms are widely used in surface alignment, because of their low computational complexity and guaranteed convergence [16]. Among them, probabilistic registration algorithm is a popular kind of state-of-the-art algorithms to solve PSR. Since a one-to-many alignment strategy is adopted, probabilistic registration algorithms achieve better performance than other conventional optimization-based registration algorithms in presence of noise and outliers. In general, probabilistic registration algorithms cast PSR into the problem of estimating the parameters of mixture model. In many previous studies, the Gaussian mixture model (GMM) and the Hybrid mixture models (HMM) both are mainstream mixture model utilized in probabilistic registration algorithms.

GMM-based registration is a mainstream method when the number of position features is considerable. In this framework, the observed PS and the model PS are described by GMM and the registration problem is treated as minimizing the L_2 distance between two Gaussian mixtures [17]. Since it is not possible to compute high-dimensional data directly in the MLE problem, the EM framework is a widely utilized optimization strategy to estimate the transformation matrix and GMM parameters. In the coherent point drift (CPD) method

This work was supported in part by Guangdong Basic and Applied Basic Research Foundation under Grant 2021A1515011964, and in part by the Science and Technology Innovation Committee of Shenzhen under Grant JCYJ20200109112818703 and GXWD20201230155427003-20200824015626001.

[1]Zhengyan Zhang, Jiaole Wang, Shuang Song are with School of Mechanical Engineering and Automation, Harbin Institute of Technology (Shenzhen), Shenzhen 518055, China.

[2]Zhe Min is with the Department of Medical Physics and Biomedical Engineering, University College London, London, United Kingdom.

[3]Ang Zhang is with the Department of Electronic Engineering, The Chinese University of Hong Kong, Hong Kong.

[4]Max Q.-H. Meng is with the Department of Electronic and Electrical Engineering, Southern University of Science and Technology, Shenzhen 518055, China.

*Corresponding authors: Jiaole Wang, mail: wangjiaole@hit.edu.cn, Shuang Song, mail: songshuang@hit.edu.cn.

†The first two authors contributed equally to this work.

[18], the GMM centroids are forced to move coherently as a group to maintain the topological structure of the PS. In the expectation conditional maximization for point registration (ECMPR) algorithm [19], three conditional maximization steps replace the traditional M-step, and the anisotropic positional covariance matrix is utilized. The jointly register multiple PSs (JRMPC) algorithm [20] considers any point as a realization of a single GMM and recast the registration problem into a cluster problem. All of these above-mentioned GMM-based approaches consider only the location features of the PS, which is feasible when the point features are sufficient.

Furthermore, a novel HMM-based registration combining multiple features such as position information and orientation has been proposed. In this framework, the correspondences between two PSs are computed according to both position and orientation information. Ravikumar *et al.* [21] have formulated an HMM consisting of Student's t and vMF distributions for group-wise registration. Min *et al.* [22] have proposed a probabilistic registration method for human femur bones, where a GPS is represented by the HMM containing a GMM and a vMF. Then, they extend this framework to nonrigid registration with anisotropic noise [23]. However, in these HMM-based algorithms, the normal vectors were pre-assumed to be available accurately and reliably at each point.

In this paper, we incorporate the partially reliable normal vectors into PSR. Normal vectors are extracted by principal component analysis (PCA) on a matrix consisting of position information of a PS [24]. The point clouds subset containing reliable normal vectors is applied to HMM. In contrast, the normal vectors extracted from the remaining points are not available or are subject to large errors. The registration problem is formulated by aligning two above-mentioned mixture models. The idea of our algorithm is then shown in Fig. 1. The EM framework is used to solve the MLE problem.

The rest of this paper is organized as follows. Section II summaries the motivations and the contributions of this papers. Section III presents the formulation of a partial observable PSR problem in a probabilistic framework. Section IV describes the details of our method. Section V presents the implementation details of experiments. Section VI discusses the proposed method and experimental results. Section VII concludes this paper.

II. Motivations and Contributions

The motivations of this paper are twofold. One is to eliminate the error caused by normal vectors estimated in the pre-operative stage. In previous studies, normal vectors can be acquired by using points of the neighborhood in the surface can estimate normal vectors from the 3D model. The virtual model is reconstructed from CT or MRI in the pre-operative stage. However, accurate estimation of normal vectors has potential challenges due to the presence of surfaces with large curvature and the non-uniform density of the points. Besides, the accuracy and robustness of surface normal estimation is sensitive to addictive and outlier noise. As is reported in [24], average orientation error per point ranges $[10, 20]^\circ$ under the Gaussian noise with $\sigma_n = 0.6\%$. The other motivation

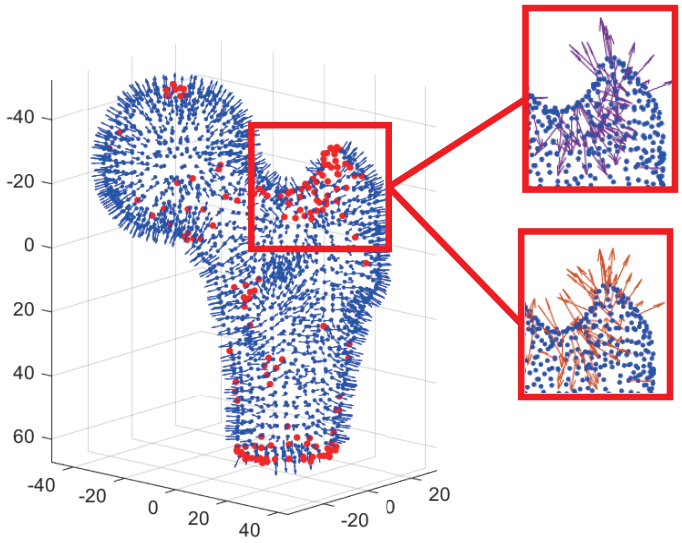

Fig. 2: PS with reliable normal vectors of the human femur bone. Red points represent point subset where the orientation information is unreliable. Blue points and associated arrows represent point subset where the orientation information is considered. Orientation estimations of two different methods are shown in two right subfigures.

is to reduce the noise and outliers produced in the intra-operative measurement. Surgeons usually use a tracked probe attached with a force sensor to measure normal vectors in the intra-operative stage. However, the measurement of normal vectors can be affected by different points, directions and magnitudes of external force. According to research [25], the measurement error and standard deviation are 0.7mm and 2.5mm respectively, when the force magnitude ranges in $[5, 40]$N. Consequently, it is a challenging work for surgeons to measure the orientation accurately in the clinic.

This paper is a significantly extended work of the HMM-based algorithm. Due to the evaluation of normal vectors, our method achieves more accurate results in PSR in computer-assisted orthopedic surgery (CAOS). The main contributions of this paper can be summarized as follows.

1) Under the HMM framework, we first introduce the proposed indicators to assess the reliability of normal vectors. The curvature of a surface is introduced to assess the reliability of normal vectors.
2) Rigid registration of two PSs with position information and partial reliable normal vectors is formally formulated as an MLE problem, which is dealt with the EM framework.
3) The proposed registration algorithm is benchmarked by comparing to the state-of-the-art probabilistic methods in terms of accuracy, noise robustness, and convergence speed. The experimental results demonstrate that the proposed method outperforms the other compared methods in different conditions.

III. Reliable Hybrid Mixture Model

In this paper, two PSs are first preprocessed before computing orientation features. To evaluate the reliability of the normal vector generated at each position, the curvature of the

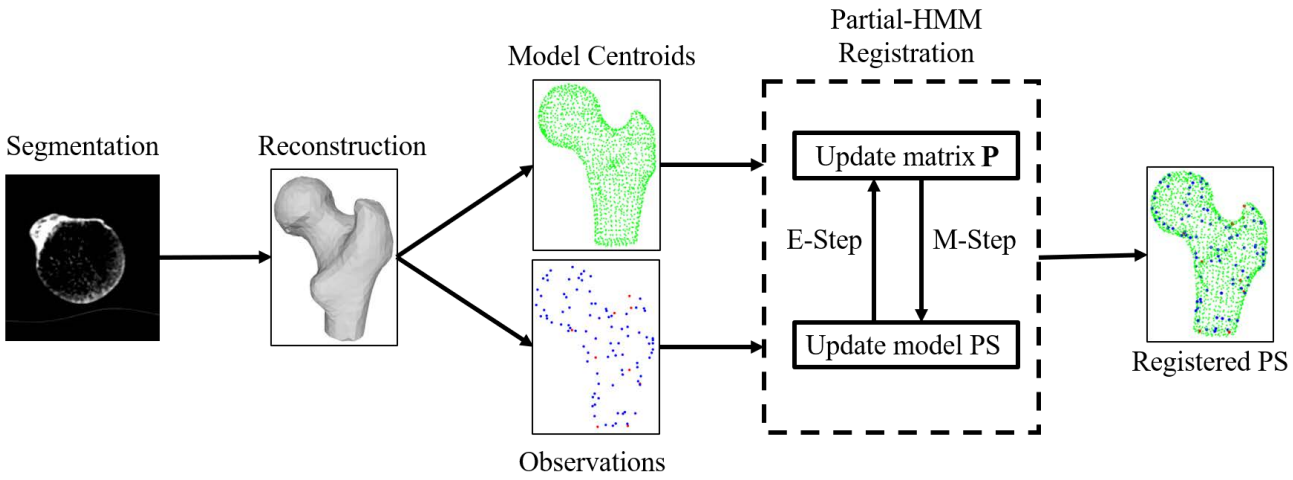

Fig. 3: Overview of our proposed PSR algorithm. The pre-operative CT is captured and segmented to create a surface representation of the anatomy (in our case, the human femur bone). This surface is then used to extract the model PS. The observed PS is also randomly sampled from this surface for simulation. The partial-HMM registration algorithm accurately aligns the model PS with the observed PS.

fitted plane is introduced as a credibility evaluation standard. Normal vectors estimated at points with small curvature of the fitted plane are deemed to be reliable. Hence, these positions and normal vectors form reliable feature subsets in the model set $(\mathbf{Y}, \hat{\mathbf{Y}})$ and the observed set $(\mathbf{X}, \hat{\mathbf{X}})$, respectively. Meanwhile, normal vectors of other points will be considered unreliable. Consequently, the normal vectors of observed and model sets can be defined as follows.

$$\begin{aligned} \hat{x}_n &= \delta_w \hat{x}_n \\ \hat{y}_m &= \delta_w \hat{y}_m \end{aligned} \tag{1}$$

where $1 \le n \le N$, $1 \le m \le M$, and δ_w is the Kronecker symbol to distinguish the reliability of normal vectors, according to the curvature of one point. The Kronecker symbol is defined as follows.

$$\delta_w = \begin{cases} 1, & \text{if } w < w_0 \\ 0, & \text{otherwise.} \end{cases} \tag{2}$$

where w denotes the curvature of one point in the observed and the model sets, w_0 denotes the threshold that distinguishes the reliability of normal vectors. The result of preprocessing is shown in Fig. 2. The observation is that red points ignoring normal vectors mainly distribute on the steep curvature of the bone surface and the edge of a surface, where orientation estimation of two different methods has large difference. This is in line with our idea of preprocessing.

After preprocessing, the registration of two PSs is further formulated as an MLE problem. More specifically, we consider the points in $\mathbf{Y}$ as the GMM centroids, and the points in $\mathbf{X}$ are generated by GMM. The unit normal vectors in the reliable observed orientation set are generated by the Fisher mixture model (FMM). The reliable normal vectors denote the mean and central directions of FMM. The position vectors and unit normal vectors are assumed to be independent. Hence, the probability density function (PDF) of the n^{th} point in the observed data set is described as following.

$$p\left(\mathbf{d}_n \middle| \Theta\right) = \sum_{m=1}^{M+1} P(z_n = m) p(\mathbf{d}_n | z_n = m; \Theta) \tag{3}$$

where $1 \le n \le N$ and Θ denotes all parameters in the mixture model. $P(z_n = m)$ is the prior probability that the n^{th} point is registered to the m^{th} point, which is defined as following.

$$P(z_n = m) = \delta_w \frac{1}{M_1} + (1 - \delta_w) \frac{1}{M_2} \tag{4}$$

where M_1 and M_2 denote the number of points in the model set that incorporate reliable normal vectors or not, respectively. In order to express the independence of position vectors and normal vectors, we define the positional and orientational PDFs as follows.

$$\begin{aligned} p_p(\mathbf{d}_n | z_n = m; \Theta) &= \frac{1}{(2\pi\sigma^2)^{\frac{3}{2}}} e^{-\frac{1}{2\sigma^2}\|\mathbf{x}_n - (\mathbf{R}\mathbf{y}_m + \mathbf{t})\|^2} \\ p_o(\mathbf{d}_n | z_n = m; \Theta) &= \left[\frac{\kappa}{2\pi(e^{\kappa} - e^{-\kappa})} e^{\kappa(\mathbf{R}\hat{\mathbf{y}}_m)^T \hat{\mathbf{x}}_n} \right]^{\delta_w} \end{aligned} \tag{5}$$

With above assumption, given all model parameters Θ and correspondence $z_n = m$, the PDF of n^{th} point with reliably direction feature is

$$p(\mathbf{d}_n | z_n = m; \Theta) = p_p(\mathbf{d}_n | z_n = m; \Theta) p_o(\mathbf{d}_n | z_n = m; \Theta) \tag{6}$$

where $1 \le n \le N$ and $1 \le m \le M$. To account for noise and outliers normally distributed in the observed PS, uniform distribution $p(\mathbf{d}_n | z_n = M+1)$ is added to the mixture model in (3). The PDF of outliers' uniform distribution is defined as follows.

$$p\left(\mathbf{d}_n \middle| z_n = M+1; \Theta\right) = \delta_w \frac{1}{N_1} + (1 - \delta_w) \frac{1}{N_2} \tag{7}$$

where N_1 and N_2 denote the number of points in the observed set that incorporate reliable normal vectors or not, respectively. Furthermore, $0 \le \omega \le 1$ represents the weight of uniform distribution. Therefore, the PDF in (3) can be written as

$$\begin{aligned} p(\mathbf{d}_n | \Theta) = {} & \omega p(\mathbf{d}_n | z_n = M+1; \Theta) \\ & + (1 - \omega) \sum_{m=1}^{M} P(z_n = m) p(\mathbf{d}_n | z_n = m; \Theta) \end{aligned} \tag{8}$$

We integrate these probabilities into optimal estimation for mixture model, by maximizing the likelihood function, or equivalently by minimizing the negative log-likelihood function as follows:

$$Q\left(\Theta\right)=f(\lambda,\delta_w)\sum_{n=1}^{N}\log\sum_{m=1}^{M+1}P(z_n=m)p(\mathbf{d}_n|\,z_n=m;\Theta) \tag{9}$$

where $f(\lambda,\delta)=\lambda\delta_w+(1-\lambda)(1-\delta_w)$ represents the choice weight function, and $\lambda=N_1/N$ represents the weight of registration considering orientation vectors.

IV. Generalized Point Set Registration by Reliable HMM

Generalized point set registration by reliable HMM adopt the EM framework to solve probabilistic optimization problem. As proposed in [18], the idea of EM is first to determine the initial value of all parameters and then compute the posterior probability of mixture components. In our algorithm, the posterior probabilities of mixture components are derived by using Bayes' theorem, which is the expectation or E-step of the algorithm. Given new posterior probability, the new model parameters can be updated by minimizing the negative log-likelihood function as following [22].

$$\begin{aligned}Q(\Theta^{new}|\,\Theta^{old})=f(\lambda,\delta)\sum_{n=1}^{N}\sum_{m=1}^{M}\big[p(z_n=m|\,\mathbf{d}_n;\Theta^{old})\\ \log\left(P(z_n=m)p(\mathbf{d}_n|\,z_n=m;\Theta^{new})\right)\big]\end{aligned} \tag{10}$$

where $P(z_n=m)$ is the prior probability computed in (4), $p(z_n=m|\,\mathbf{d}_n;\Theta^{old})$ is computed in the E-step, and $p(\mathbf{d}_n|\,z_n=m;\Theta^{new})$ is derived in (6). We define (10) as the objective function, which is the upper bound of the negative log-likelihood function in (9). By using properties of logarithmic functions and ignoring the parameters unrelated to Θ, the objective function can be expanded as follows:

$$\begin{aligned}&Q(\Theta^{new}|\,\Theta^{old})\\&=f(\lambda,\delta_w)\sum_{n=1}^{N}\sum_{m=1}^{M}p_{mn}\frac{1}{2\sigma^2}\|\mathbf{x}_n-(\mathbf{R}\mathbf{y}_m+\mathbf{t})\|^2\\&-\lambda\delta_w\sum_{n=1}^{N}\sum_{m=1}^{M}p_{mn}\cdot\kappa(\mathbf{R}\hat{\mathbf{y}}_m)^T\hat{\mathbf{x}}_n\\&+N_p\left[\log\kappa-\log\left(e^{\kappa}-e^{-\kappa}\right)+\frac{3}{2}\log\sigma^2\right]\end{aligned} \tag{11}$$

where we define $N_p=f\left(\lambda,\delta_w\right)\sum_{n=1}^{N}\sum_{m=1}^{M}p_{mn}$, and p_{mn} is abbreviations of $p(z_n=m|\,\mathbf{d}_n;\Theta^{old})$ computed in the E-step. For clarity, the flow chart of our algorithm is summarized in Fig. 3.

A. E-Step

In the E-step, posterior probabilities of mixture components are computed by Bayes' theorem.

$$p\left(z_n=m|\,\mathbf{d}_n;\Theta^{old}\right)=\frac{P(z_n=m)p(\mathbf{d}_n|\,z_n=m;\Theta^{old})}{p(\mathbf{d}_n|\,\Theta^{old})} \tag{12}$$

where $p\left(\mathbf{d}_n|\,z_n=m;\Theta^{old}\right)$ and $p(\mathbf{d}_n|\,\Theta^{old})$ are computed in (6) and (8) respectively.

B. M-Rigid Step

In this step, given new posteriors and old model parameters, the transformation matrix $[\mathbf{R},\mathbf{t}]$ can be optimized by minimizing the objective function. First, to find the optimal vector $\mathbf{t}^*$, the parameters independent of $\mathbf{t}$ are ignored. The optimization function can be simplified as follows:

$$\mathbf{t}^*=\arg\min_{\mathbf{t}}\frac{f\left(\lambda,\delta_w\right)}{2\sigma^2}\sum_{n=1}^{N}\sum_{m=1}^{M}p_{mn}\|\mathbf{x}_n-(\mathbf{R}\mathbf{y}_m+\mathbf{t})\|^2 \tag{13}$$

Then $\mathbf{t}^*$ can derived by solving $\partial Q(\Theta^{new}|\,\Theta^{old})/\partial\mathbf{t}=0$, that is

$$\frac{\partial}{\partial\mathbf{t}}\left[\frac{f\left(\lambda,\delta_w\right)}{2\sigma^2}\sum_{n=1}^{N}\sum_{m=1}^{M}p_{mn}\|\mathbf{x}_n-(\mathbf{R}\mathbf{y}_m+\mathbf{t})\|^2\right]=0 \tag{14}$$

We can obtain

$$\mathbf{t}^*=\mu_x-\mathbf{R}\mu_y \tag{15}$$

where μ_x and μ_y can be represented as following:

$$\begin{cases}\mu_x=\frac{1}{N_p}f\left(\lambda,\delta_w\right)\mathbf{X}^T\mathbf{P}^T\mathbf{1}\\ \mu_y=\frac{1}{N_p}f\left(\lambda,\delta_w\right)\mathbf{Y}^T\mathbf{P}\mathbf{1}\end{cases} \tag{16}$$

where A^T denotes the transpose of a matrix or vector and $\mathbf{P}$ is a posterior matrix composed of posterior probabilities p_{mn}.

To find the optimal rotation matrix $\mathbf{R}^*$, we let the partial derivative of the objective function concerning $\mathbf{R}$ be equal to zero. By eliminating the parameters independent of $\mathbf{R}$, the optimization equation can be deduced as follows:

$$\begin{aligned}\mathbf{R}^*=\arg\max_{\mathbf{R}}\Bigg[&\frac{f\left(\lambda,\delta_w\right)}{2\sigma^2}\sum_{n=1}^{N}\sum_{m=1}^{M}p_{mn}\left\|\mathbf{x}_n-(\mathbf{R}\mathbf{y}_m+\mathbf{t})\right\|\\&+\lambda\delta_w\sum_{n=1}^{N}\sum_{m=1}^{M}p_{mn}\kappa(\mathbf{R}\hat{\mathbf{y}}_m)^T\hat{\mathbf{x}}_n\Bigg]\end{aligned} \tag{17}$$

By substituting $\mathbf{t}$ with $\mathbf{t}^*$, we have

$$\begin{aligned}\mathbf{R}^*=\arg\max_{\mathbf{R}}\Bigg[&\frac{f\left(\lambda,\delta_w\right)}{\sigma^2}\sum_{n=1}^{N}\sum_{m=1}^{M}p_{mn}\mathbf{x}_n^{'T}\mathbf{R}\mathbf{y}_m^{'}\\&+\lambda\delta_w\sum_{n=1}^{N}\sum_{m=1}^{M}p_{mn}\kappa(\mathbf{R}\hat{\mathbf{y}}_m)^T\hat{\mathbf{x}}_n\Bigg]\end{aligned} \tag{18}$$

where $\mathbf{x}_n^{'}=\mathbf{x}_n-\mu_x$ and $\mathbf{y}_n^{'}=\mathbf{y}_n-\mu_y$. By using $\mathbf{H}_1$ and $\mathbf{H}_2$, we can obtain

$$\begin{aligned}\mathbf{R}^*&=\arg\max_{\mathbf{R}}Tr\left(\mathbf{H}_1\mathbf{R}+\mathbf{H}_2\mathbf{R}\right)\\&=\arg\max_{\mathbf{R}}Tr\left(\mathbf{H}\mathbf{R}\right)\end{aligned} \tag{19}$$

where $Tr\left(\bullet\right)$ denotes the trace of matrix. Then optimal rotation matrix can be got as following:

$$\mathbf{R}^*=\mathbf{U}diag(1,1,\det(\mathbf{U}\mathbf{V}^T))\mathbf{V}^T \tag{20}$$

where $diag\left(\mathbf{A}\right)$ denotes the diagonal matrix consisting of elements in the $\mathbf{A}$. $\mathbf{U}$ and $\mathbf{V}$ can be found by singular value decomposition (SVD) of $\mathbf{H}^{\mathbf{T}}$.

C. M-Var Step

Then, given the newly updated transform matrix, the optimization problem concerning the variance of the Gaussian distribution σ^2 is following:

$$\left(\sigma^2\right)^* = \arg\min_{\sigma^2} \left[\frac{f\left(\lambda, \delta_w\right)}{2\sigma^2} \sum_{n=1}^{N} \sum_{m=1}^{M} p_{mn} \|\mathbf{x}_n - (\mathbf{R}^* \mathbf{y}_m + \mathbf{t}^*)\|^2 + \frac{3}{2} N_p \log \sigma^2 \right] \tag{21}$$

Letting the partial derivative of the objective function concerning σ^2 be equal to zero, we have

$$\left(\sigma^2\right)^* = \frac{f\left(\lambda, \delta_w\right) \sum_{n=1}^{N} \sum_{m=1}^{M} p_{mn} \|\mathbf{x}_n - (\mathbf{R}^* \mathbf{y}_m + \mathbf{t}^*)\|^2}{3 N_p} \tag{22}$$

D. M-Con Step

Afterwards, given the updated transformation matrix $[\mathbf{R}, \mathbf{t}]$ and new variance of mixture model, the optimization function with respect to the concentration parameter of von-Mises-Fisher distribution κ can be deduced as following:

$$\kappa^* = \arg\min_{\sigma^2} \left[\lambda \delta_w \sum_{n=1}^{N} \sum_{m=1}^{M} p_{mn} \kappa (\mathbf{R}\hat{\mathbf{y}}_m)^T \hat{\mathbf{x}}_n - N_p \log \kappa + N_p \log(e^{\kappa} - e^{-\kappa}) \right] \tag{23}$$

Then the new κ can be obtained by solving the equation that partial derivative of the objective function concerning κ equals zero.

$$\frac{1}{\kappa} = \frac{e^{\kappa} + e^{-\kappa}}{e^{\kappa} - e^{-\kappa}} - \frac{\lambda \delta_w}{N_p} \sum_{n=1}^{N} \sum_{m=1}^{M} p_{mn} (\mathbf{R}\hat{\mathbf{y}}_m)^T \hat{\mathbf{x}}_n \tag{24}$$

Then the new κ is updated by solving this nonlinear equation.

E. M-Model Step

In this step, the new model set including positions and normal vectors is updated, by using new $\mathbf{R}^*$ and $\mathbf{t}^*$.

$$\begin{aligned} \mathbf{Y}^{new} &= \mathbf{R}^* \mathbf{Y}^{old} + \mathbf{t}^* \\ \hat{\mathbf{Y}}^{new} &= \mathbf{R}^* \hat{\mathbf{Y}}^{old} \end{aligned} \tag{25}$$

where $\mathbf{R}^*$ and $\mathbf{t}^*$ are updated in Section IV-B. The proposed algorithm is summarized in Algorithm 1.

Algorithm 1: Generalized Point Set Registration by Reliable HMM

Input: Point clouds set $(\mathbf{X}, \hat{\mathbf{X}})$ and $(\mathbf{Y}, \hat{\mathbf{Y}})$
Output: Transform matrix $\mathbf{R}^*$ and $\mathbf{t}^*$
Initialization: Initialize $\mathbf{\Theta}|^0 = \left\{ \mathbf{R}|^0, \mathbf{t}|^0, \kappa|^0, \sigma^2\big|^0 \right\}$
while *not convenged* **do**
  1) E-step: Compute posterior probability matrixes $\mathbf{P}$ in (12), given current $\left\{\mathbf{R}, \mathbf{t}, \kappa, \sigma^2\right\}$
  2) M-rigid step: Update $\mathbf{R}$ and $\mathbf{t}$ in (20) and (15)
  3) M-var step: Update σ^2 in (22)
  4) M-con step: Update κ in (24)
  5) M-model step: Update the new model set $(\mathbf{Y}, \hat{\mathbf{Y}})$ in (25)
end
Return: $\mathbf{R}^*$ and $\mathbf{t}^*$

V. Implementation Details

Since the EM algorithm is sensitive to the initial value, the pre-determinations of parameters' value are necessary. We experientially initialize the number of $\kappa|^0$ to be 1 and the initial variance is set as $\sigma^2\big|^0 = \sum_{n=1}^{N} \sum_{m=1}^{M} \|\mathbf{x}_n - \mathbf{y}_m\|^2 \big/ 3MN$. The weight ω in (8) is set to be 0.5. Considering that the two PSs are not aligned at the beginning of the iterative algorithm, the initial transformation matrix is set as $\mathbf{R}|^0 = \mathbf{I}_{3\times3}$, $\mathbf{t}|^0 = \mathbf{0}_{3\times1}$. As the iteration proceeds, the value of σ^2 tends more and more to zero and the value of κ becomes larger. However, the increase in the value of κ will result in the number of e^{κ} become larger. Hence, we set the upper bound of κ to be 100. The iterative algorithm will stop if one of three following convergence conditions is satisfied: 1) the value of σ^2 is less than 10^{-4}; 2) the rate of the change of σ^2 is less than 10^{-6}; 3) the number of iterations reaches 100.

VI. Results and Discussion

Two experiments on the human femur bone model are conducted to validate the proposed algorithm. All experiments are done on a surface PS on a human femur bone segmented from the CT image. The model PS $(\mathbf{Y}, \hat{\mathbf{Y}})$ has 1586 points and the observed PS $(\mathbf{X}, \hat{\mathbf{X}})$ are randomly sampled from the model PS. To highlight the advantage of the proposed algorithm, two different ratios of unreliable normal vectors in the model PS are set in the following experiment. In the model PS, the normal vectors of the points with curvature ranking in the top 75% and 90% are considered to be reliable in the experiment, respectively. The rest of normal vectors are considered to be wrong. For each experiment, 100 registration trials are conducted to compare our algorithm with ECMPR and original HMM. For every trial, the true rotation matrix $\mathbf{R}_{true}$ and translation vector $\mathbf{t}_{true}$ are randomly generated from $[10, 20]^{\circ}$ and $[10, 20]$mm. Then the transform matrix is applied to $(\mathbf{X}, \hat{\mathbf{X}})$ to obtain misaligned observed data set, which is motivated to simulate practical clinical applications. The estimated transform matrix is represented as $[\mathbf{R}_{cal}, \mathbf{t}_{cal}]$. Two kinds of noise were injected into data, including position noise obeying Gaussian distribution and orientation noise obeying vMF distribution. We set two levels noise for positions and unit normal vectors in $(\mathbf{X}, \hat{\mathbf{X}})$: $\mu = 0, \sigma^2 = 1/3, \kappa = 800$ and $\mu = 0, \sigma^2 = 4/3, \kappa = 3200$. Errors of the transform matrix can be represented as follows: $error_{\mathbf{R}} = \|\mathbf{R}_{true} - \mathbf{R}_{cal}\|$ and $error_{\mathbf{t}} = \|\mathbf{t}_{true} - \mathbf{t}_{cal}\|$.

A. Experiment I: Outliers Robustness

In this section, the robustness of three algorithms to different numbers of outliers is tested. The number of inlier points in $(\mathbf{X}, \hat{\mathbf{X}})$ was set to be 100. The generation of outliers has two steps. Firstly, the positional vectors were generated by randomly translating observed points with random vectors whose lengths ranged in $[10, 20]$mm. Secondly, the orientational vectors were randomly generated within $[0, 360]^{\circ}$.

TABLE I: P-value of the statistical tests comparing the error results using the proposed algorithm and the other two algorithms in experiment I. Rot and Trans are used as the abbreviation for rotational error and translational error respectively. The table (a) presents p-values of results when the ratio of reliable normal vectors in the model PS is set 90%. The table (b) presents p-values of results when the ratio of reliable normal vectors in the model PS is set 75%.

(a) The ratio of reliable normal vectors: 90%

	Low Noise				High Noise			
Outlier Percentage	ECMPR(Rot)	HMM(Rot)	ECMPR(Trans)	HMM(Trans)	ECMPR(Rot)	HMM(Rot)	ECMPR(Trans)	HMM(Trans)
10%	9.11×10^{-10}	3.41×10^{-15}	6.03×10^{-12}	2.42×10^{-15}	1.66×10^{-12}	7.04×10^{-13}	1.48×10^{-15}	1.42×10^{-7}
20%	9.69×10^{-35}	1.11×10^{-8}	8.88×10^{-19}	2.05×10^{-14}	9.04×10^{-30}	5.56×10^{-13}	4.49×10^{-6}	1.66×10^{-16}
30%	1.73×10^{-33}	1.10×10^{-8}	6.44×10^{-29}	1.31×10^{-9}	9.22×10^{-34}	1.63×10^{-11}	2.28×10^{-15}	1.06×10^{-18}
40%	2.44×10^{-46}	0.0138	7.99×10^{-48}	0.0219	9.52×10^{-46}	6.04×10^{-7}	8.50×10^{-34}	6.46×10^{-14}
50%	2.36×10^{-54}	2.03×10^{-5}	3.95×10^{-54}	**0.6342**	3.16×10^{-58}	1.40×10^{-5}	1.37×10^{-49}	2.03×10^{-10}

(b) The ratio of reliable normal vectors: 75%

	Low Noise				High Noise			
Outlier Percentage	ECMPR(Rot)	HMM(Rot)	ECMPR(Trans)	HMM(Trans)	ECMPR(Rot)	HMM(Rot)	ECMPR(Trans)	HMM(Trans)
10%	6.00×10^{-11}	5.68×10^{-13}	1.66×10^{-9}	1.18×10^{-23}	1.13×10^{-12}	4.99×10^{-15}	3.29×10^{-15}	5.34×10^{-5}
20%	3.57×10^{-16}	1.21×10^{-26}	1.41×10^{-15}	0.0138	2.43×10^{-31}	1.04×10^{-23}	0.0032	**0.56**
30%	4.57×10^{-24}	1.12×10^{-39}	3.44×10^{-27}	3.12×10^{-42}	2.56×10^{-36}	4.86×10^{-33}	1.55×10^{-14}	4.12×10^{-20}
40%	9.31×10^{-43}	1.38×10^{-12}	2.47×10^{-51}	3.31×10^{-52}	3.21×10^{-49}	4.92×10^{-34}	9.69×10^{-34}	1.24×10^{-16}
50%	3.24×10^{-39}	2.00×10^{-33}	9.96×10^{-62}	9.21×10^{-48}	1.00×10^{-63}	7.92×10^{-34}	1.69×10^{-52}	9.95×10^{-17}

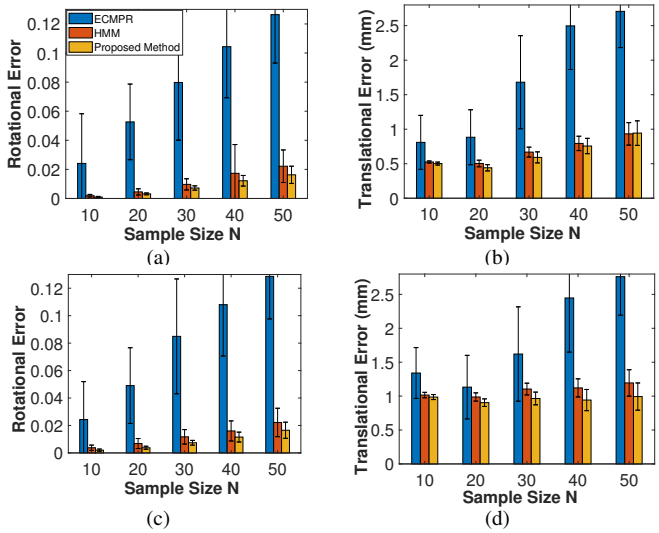

Fig. 4: Four plots represent the rotational and translational errors' means and standard deviations under five different numbers of injected outliers and different noise in Experiment I. In this experiment, the ratio of reliable normal vectors in the model PS is set as 90%. (a) Low noise, rotational error. (b) Low noise, translational error. (c) High noise, rotational error. (d) High noise, translational error.

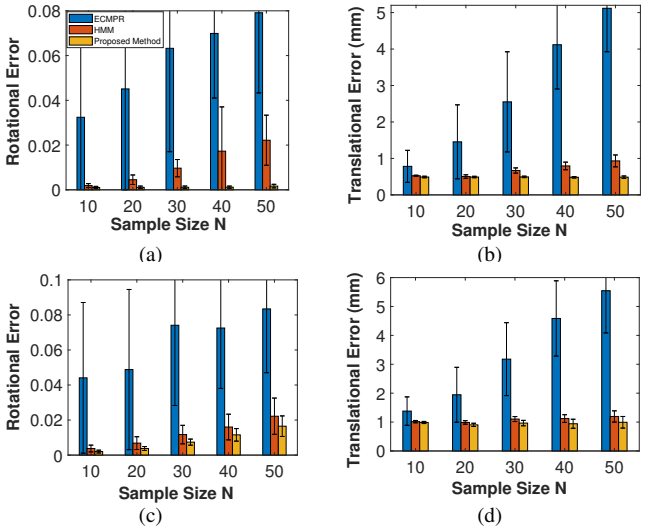

Fig. 5: Four plots represent the rotational and translational errors' means and standard deviations under five different numbers of injected outliers and different noise in Experiment I. In this experiment, the ratio of reliable normal vectors in the model PS is set as 75%. (a) Low noise, rotational error. (b) Low noise, translational error. (c) High noise, rotational error. (d) High noise, translational error.

For each trial, five different ratios of outliers were set to be $10\% \sim 50\%$, which means the number of points in the observed PS ranges in $[110, 150]$.

1) 90% reliability: Fig. 4 shows the rotational errors and the corresponding translational errors of three algorithms in cases where five different percentages of outliers were injected under two levels of noise, respectively. In the experiment shown in Fig. 4, the ratio of reliable normal vectors in the model PS is set as 90%. As shown in Fig. 4(a) and (c), the means of rotational errors of our algorithm are less than ECMPR and original HMM. With more outliers injected in the observed PS, our algorithm achieves better results than ECMPR and original HMM.

2) 75% reliability: Fig. 5 shows the rotational errors and the corresponding translational errors of three algorithms in cases where five different percentages of outliers were injected under two levels of noise, respectively. In the experiment shown in Fig. 5, the ratio of reliable normal vectors in the model PS is set as 75% . As shown in Fig. 5, both rotational errors and translational errors of our algorithm are less than ECMPR and original HMM. Comparing Fig. 4 and Fig. 5, the observation can be obtained that ignoring more unreliable normal vectors in the model PS can effectively reduce errors and improve robustness, compared with original HMM. Especially under high noise, the means of translational error are less than 1 mm, which is considered to meet the clinical

TABLE II: P-value of the statistical tests comparing the error results using the proposed algorithm and the other two algorithms in experiment II. Rot and Trans are used as the abbreviation for rotational error and translational error respectively. The table (a) presents p-values of results when the ratio of reliable normal vectors in the model PS is set 90%. The table (b) presents p-values of results when the ratio of reliable normal vectors in the model PS is set 75%.

(a) The ratio of reliable normal vectors: 90%

	Low Noise				High Noise			
Outlier Percentage	ECMPR(Rot)	HMM(Rot)	ECMPR(Trans)	HMM(Trans)	ECMPR(Rot)	HMM(Rot)	ECMPR(Trans)	HMM(Trans)
3	6.71×10^{-20}	0.0019	2.64×10^{-29}	1.64×10^{-7}	1.10×10^{-23}	8.57×10^{-7}	0.0292	2.70×10^{-4}
5	1.09×10^{-4}	5.18×10^{-14}	1.63×10^{-4}	**0.0927**	8.98×10^{-8}	7.36×10^{-17}	5.33×10^{-6}	0.0051
7	7.18×10^{-7}	1.02×10^{-19}	9.38×10^{-6}	1.64×10^{-7}	2.70×10^{-9}	3.05×10^{-19}	1.10×10^{-7}	2.46×10^{-10}
9	2.13×10^{-5}	4.67×10^{-13}	2.00×10^{-4}	3.77×10^{-18}	1.75×10^{-6}	6.41×10^{-16}	0.0020	**0.0737**

(b) The ratio of reliable normal vectors: 75%

	Low Noise				High Noise			
Outlier Percentage	ECMPR(Rot)	HMM(Rot)	ECMPR(Trans)	HMM(Trans)	ECMPR(Rot)	HMM(Rot)	ECMPR(Trans)	HMM(Trans)
3	9.40×10^{-24}	0.0348	7.66×10^{-25}	1.08×10^{-11}	4.65×10^{-24}	9.13×10^{-19}	5.05×10^{-5}	2.37×10^{-31}
5	4.04×10^{-8}	3.15×10^{-11}	3.04×10^{-40}	3.74×10^{-5}	6.39×10^{-8}	3.68×10^{-37}	4.47×10^{-5}	2.62×10^{-26}
7	7.12×10^{-10}	2.49×10^{-53}	3.86×10^{-25}	2.56×10^{-64}	8.82×10^{-11}	6.40×10^{-36}	8.03×10^{-7}	1.16×10^{-36}
9	4.00×10^{-7}	1.31×10^{-16}	3.08×10^{-31}	1.26×10^{-8}	8.52×10^{-7}	6.01×10^{-35}	0.0019	3.36×10^{-25}

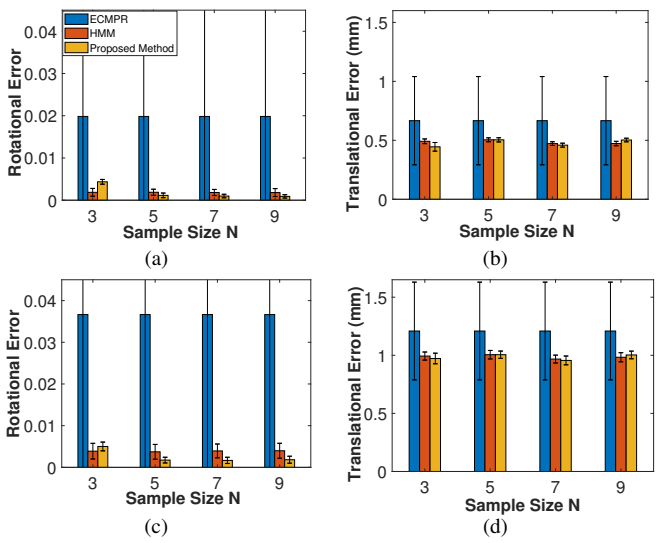

Fig. 6: Four plots represent the rotational and translational errors' means and standard deviations under five different numbers of points ignoring orientation information and different noise in Experiment II. In this experiment, the ratio of reliable normal vectors in the model PS is set as 90%. (a) Low noise, rotational error. (b) Low noise, translational error. (c) High noise, rotational error. (d) High noise, translational error.

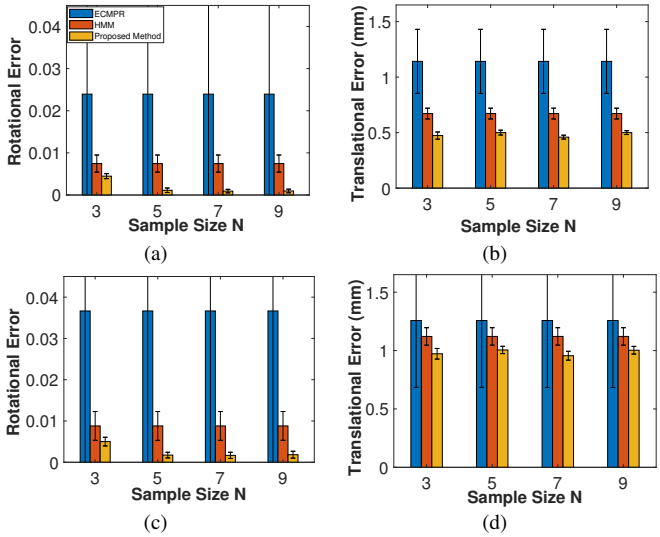

Fig. 7: Four plots represent the rotational and translational errors' means and standard deviations under five different numbers of points ignoring orientation information and different noise in Experiment II. In this experiment, the ratio of reliable normal vectors in the model PS is set as 75%. (a) Low noise, rotational error. (b) Low noise, translational error. (c) High noise, rotational error. (d) High noise, translational error.

criteria. Hence, the robustness of our proposed algorithm to outliers outperforms other algorithms in the estimation of the transformation matrix.

To verify the statistical significance of results in this experiment, Table I(a) and (b) shows the p-value of two-tailed paired t-test for two levels noise when the ratio of reliable normal vectors is set as 90% and 75%, respectively. Most p-values are less than 0.05 ($\alpha = 0.05$ significance level), indicating that the results of different algorithms in this experiment are statistically significant and have not occurred by chance.

B. Experiment II: Different numbers of points with unreliable normal vectors

In this experiment, we chose different numbers of points without incorporating normal vectors in the observed PS to validate the performance of our algorithm. The number of points in $(\mathbf{X}, \hat{\mathbf{X}})$ was set to be 100. Four different numbers of points with unreliable normal vectors in the observed PS were set as 3, 5, 7, 9.

1) 90% reliability: Fig. 6 shows the rotational errors and the corresponding translational errors of three algorithms with respect to different numbers of unreliable-orientation points under different levels noise, respectively. In the experiment shown in Fig. 6, the ratio of reliable normal vectors in the model PS is set as 90%. The mean value of the rotational error using our algorithm approximates half of that using HMM. The further observation is that the error decreases as the number of unreliable orientation points increases, within a certain range.

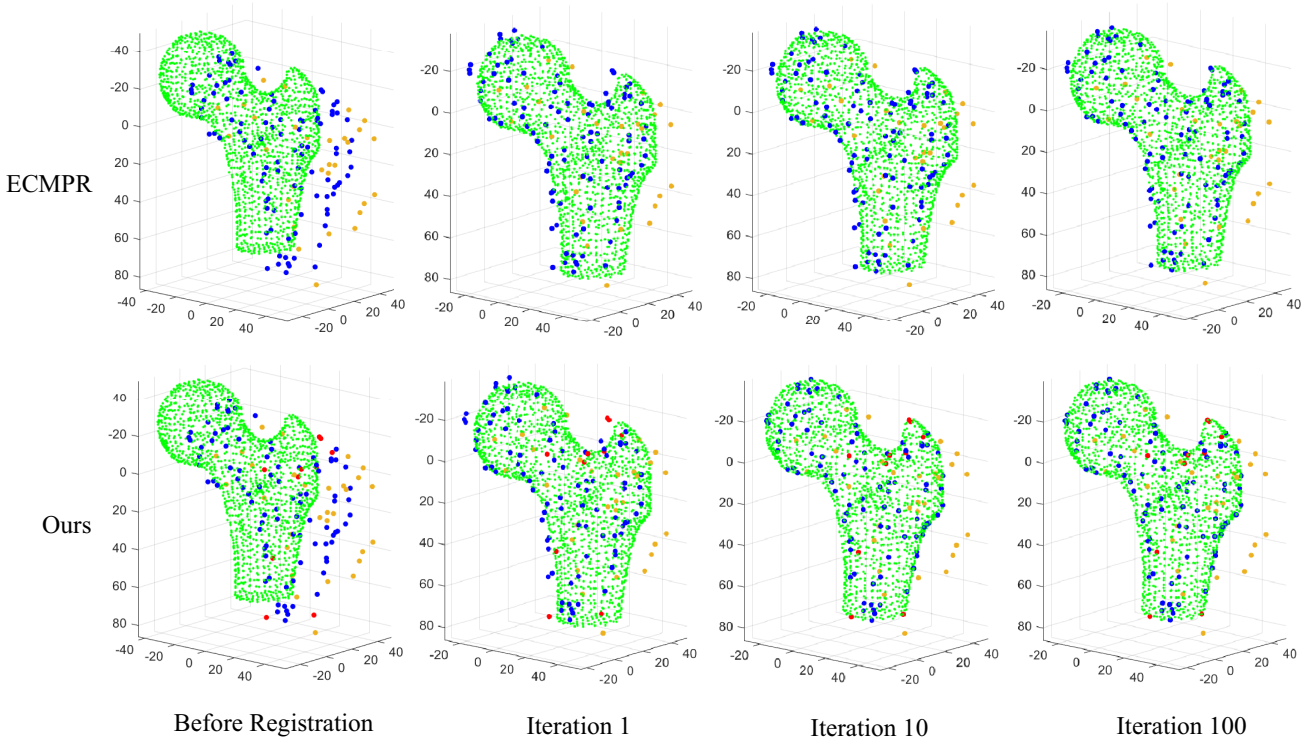

Fig. 8: Subfigures in the first and second row represent four registration results using ECMPR and our algorithm before registration and after 1, 10, 100 iterations. The low level noise and 30% outliers were injected into the observed PS. The points in the model set, points in the observed set, and outliers are shown by green, blue, and orange dots, respectively. Particularly, the points ignoring orientation information in the proposed algorithm are shown by red dots.

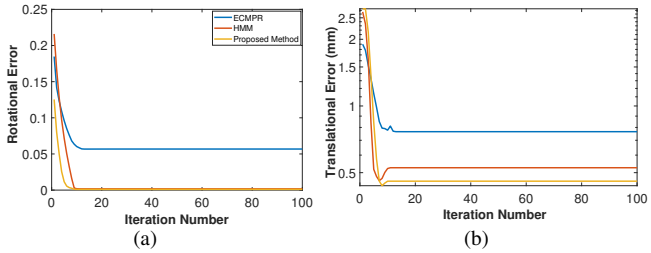

(a) (b)

Fig. 9: Convergence numbers and errors of three algorithms.

2) 75% reliability: Fig. 7 shows the rotational errors and the corresponding translational errors of three algorithms with respect to different numbers of unreliable-orientation points under different levels noise, respectively. In the experiment shown in 7, the ratio of reliable normal vectors in the model PS is set as 75%. According to Fig. 6 and 7, the proposed algorithm achieves the lowest and most robust error mean and standard deviation. As is shown in Fig. 7, when the more unreliable normal vectors in the model PS are ignored, the advantages of the proposed algorithm are more obvious. Furthermore, the proposed algorithm achieves better rotational error than the other two algorithms, with more unreliable normal vectors ignored in the observed PS.

The p-values reported in Table II also verify that the experiment results are statistically significant and that the errors of three algorithms are highly differentiated. Therefore, we can conclude that incorporating reliable normal vectors in the observed PS achieves more accurate and reliable results than that of ECMPR and original HMM.

Fig. 8 shows the registration results using ECMPR and our algorithm after four different iterations when 30% outliers were injected into the observed PS. As shown in Fig. 8, after the tenth iteration, our algorithm can well register PSs. On the contrary, the result of ECMPR algorithm is not accurate enough, after the hundredth iteration.

C. Convergence speed

Fig. 9 shows the convergence speed under the same conditions, including noise, outliers, and the number of points with unreliable orientation. As shown in Fig. 9, (1) the convergence speed of the proposed algorithm is faster than others; (2) our algorithm achieves smaller error values among the three mentioned algorithms.

D. Discussion

In this paper, we propose a novel probability-based registration algorithm that considers reliable normal vectors of PSs. The evaluation of the reliability of normal vectors is introduced into the registration algorithm. This process is more applicable for registration in the case where the PS is sparse and bears large curvature.

Extensive experimental results demonstrate that the proposed algorithm achieves improved accuracy, robustness, and convergence speed compared to the state-of-the-art methods. The benefit of incorporating normal vectors can be shown by comparing the results of ECMPR and original HMM, ECMPR and our algorithm in three experiments. More importantly, the benefit of considering the reliability of normal vectors can be validated by comparing the performance of HMM and ours

in three experiments. We emphasize again that the reliable normal vectors benefit significantly registration under different conditions. In order to better analyze the superiority of the proposed algorithm over HMM and ECMPR, the comparisons of negative-log likelihood functions of the three approaches are given as follows.

1) *Comparisons With HMM:* In HMM algorithm, normal vectors of all points are incorporated. With the model components $\Theta_{HMM} = \left\{\mathbf{R}, \mathbf{t}, \sigma^2, \kappa\right\}$, the objective function of HMM algorithm is as follows.

$$\begin{aligned} &Q(\Theta) = \\ &\sum_{n=1}^{N}\sum_{m=1}^{M} p_{mn}\left(\frac{1}{2\sigma^2}\|\mathbf{x}_n - (\mathbf{R}\mathbf{y}_m + \mathbf{t})\|^2 - \kappa(\mathbf{R}\hat{\mathbf{y}}_m)^T\hat{\mathbf{x}}_n\right) \\ &+ \frac{3}{2}N_p \log\sigma^2 + N_p \log\left(e^{\kappa} - e^{-\kappa}\right) - N_p \log\kappa \end{aligned} \tag{26}$$

Comparing (11) and (26), We can conclude that HMM algorithm has the potential to introduce wrong normal vectors on sparsely distributed point clouds. These wrong normal vectors inevitably result in poor accuracy.

2) *Comparisons With ECMPR:* In the ECMPR algorithm, the positional information of points is only considered. With the model components $\Theta_{ECMPR} = \left\{\mathbf{R}, \mathbf{t}, \sigma^2\right\}$, the objective function of ECMPR algorithm is as following.

$$Q(\Theta) = \sum_{n=1}^{N}\sum_{m=1}^{M}\frac{1}{2\sigma^2}\|\mathbf{x}_n - (\mathbf{R}\mathbf{y}_m + \mathbf{t})\|^2 + \frac{3}{2}N_p \log\sigma^2 \tag{27}$$

Comparing (11) and (27), We can conclude that the ECMPR algorithm does not take advantage of normal vectors. Therefore, registration can not achieve an accurate result when point clouds distribute sparsely.

To conclude, our algorithm brings great benefits in practical applications, especially in hip replacement surgery or pedicle screw placement. However, as the extended work of HMM, our limitations are evident. First, in our algorithm, the model PS is assumed to be noise-free, and the observed data set is sampled from it. To improve this ideal assumption, two PSs should be considered to contain noise. On the other hand, our algorithm belongs to the probabilistic registration method. Hence, our algorithm is sensitive to initial parameter such as $\sigma^2\big|^0$ and $\kappa\big|^0$.

In the future, we plan to extend our registration method by using deep learning technology to solve the above-mentioned challenges. First, the neural network will be used to estimate the normal vectors in the pre-operative stage to improve the reliability of normal vectors. Second, the registration will be considered as an end-to-end framework by the combination of neural network and optimization. In this framework, the neural network will be used to learn point-to-distribution parameter correspondences. Then these correspondences will be fed into optimization module to estimate the rigid transformation matrix.

VII. Conclusion

This paper presents a novel PSR algorithm that incorporates the concept of reliable normal vectors under the HMM framework. The proposed algorithm is validated through extensive experiments, whose results show the advantages of our algorithm in terms of accuracy, convergence speed, and robustness to the different levels of noise and outliers. Hence, the proposed algorithm is more suitable in the surface registration between pre-operative and intra-operative space, especially in the hip replacement surgery and pedicle screw placement where many fitted planes exist large curvature. In the future, we plan to combine the conventional probabilistic registration theory with deep neural networks to estimate the transformation matrix in CAOS.

References

[1] Z. Min, J. Wang, and M. Q.-H. Meng, "Robust generalized point cloud registration with orientational data based on expectation maximization," *IEEE Transactions on Automation Science and Engineering*, vol. 17, no. 1, pp. 207–221, 2020.

[2] Y. Guo, M. Bennamoun, F. Sohel, M. Lu, and J. Wan, "An integrated framework for 3-d modeling, object detection, and pose estimation from point-clouds," *IEEE Transactions on Instrumentation and Measurement*, vol. 64, no. 3, pp. 683–693, 2015.

[3] Y. Wang, Y. Liu, Q. Xie, Q. Wu, X. Guo, Z. Yu, and J. Wang, "Density-invariant registration of multiple scans for aircraft measurement," *IEEE Transactions on Instrumentation and Measurement*, vol. 70, pp. 1–15, 2021.

[4] J. Ma, J. Wu, J. Zhao, J. Jiang, H. Zhou, and Q. Z. Sheng, "Nonrigid point set registration with robust transformation learning under manifold regularization," *IEEE transactions on neural networks and learning systems*, vol. 30, no. 12, pp. 3584–3597, 2018.

[5] J. Wang, B. Tao, Z. Gong, W. Yu, and Z. Yin, "A mobile robotic 3-d measurement method based on point clouds alignment for large-scale complex surfaces," *IEEE Transactions on Instrumentation and Measurement*, pp. 1–1, 2021.

[6] J. Ge, J. Li, Y. Peng, H. Lu, S. Li, H. Zhang, C. Xiao, and Y. Wang, "Online 3-d modeling of complex workpieces for the robotic spray painting with low-cost rgb-d cameras," *IEEE Transactions on Instrumentation and Measurement*, vol. 70, pp. 1–13, 2021.

[7] M. Cao, P. Su, H. Chen, S. Tang, and Y. Liu, "3-d dense rangefinder sensor with a low-cost scanning mechanism," *IEEE Transactions on Instrumentation and Measurement*, vol. 70, pp. 1–11, 2021.

[8] Z. Min, L. Liu, and M. Q.-H. Meng, "Generalized non-rigid point set registration with hybrid mixture models considering anisotropic positional uncertainties," in *International Conference on Medical Image Computing and Computer-Assisted Intervention*. Springer, 2019, pp. 547–555.

[9] Z. Min, J. Wang, J. Pan, and M. Q.-H. Meng, "Generalized 3-d point set registration with hybrid mixture models for computer-assisted orthopedic surgery: From isotropic to anisotropic positional error," *IEEE Transactions on Automation Science and Engineering*, 2020.

[10] S. Karthick and S. Maniraj, "Different medical image registration techniques: a comparative analysis," *Current Medical Imaging*, vol. 15, no. 10, pp. 911–921, 2019.

[11] S. Shirmohammadi, K. Barbe, D. Grimaldi, S. Rapuano, and S. Grassini, "Instrumentation and measurement in medical, biomedical, and healthcare systems," *IEEE Instrumentation Measurement Magazine*, vol. 19, no. 5, pp. 6–12, 2016.

[12] D. Ottacher, A. Chan, E. Parent, and E. Lou, "Positional and orientational accuracy of 3-d ultrasound navigation system on vertebral phantom study," *IEEE Transactions on Instrumentation and Measurement*, vol. 69, no. 9, pp. 6412–6419, 2020.

[13] L. Ma, Z. Fan, G. Ning, X. Zhang, and H. Liao, "3d visualization and augmented reality for orthopedics," *Intelligent Orthopaedics*, pp. 193–205, 2018.

[14] X. Zhang, T. Wang, X. Zhang, Y. Zhang, and J. Wang, "Assessment and application of the coherent point drift algorithm to augmented reality surgical navigation for laparoscopic partial nephrectomy," *International journal of computer assisted radiology and surgery*, vol. 15, no. 6, pp. 989–999, 2020.

[15] W. Jiang, L. Ma, B. Zhang, Y. Fan, X. Qu, X. Zhang, and H. Liao, "Evaluation of the 3d augmented reality–guided intraoperative positioning of dental implants in edentulous mandibular models." *International Journal of Oral & Maxillofacial Implants*, vol. 33, no. 6, 2018.

[16] S.-Y. Guan, T.-M. Wang, C. Meng, and J.-C. Wang, "A review of point feature based medical image registration," *Chinese Journal of Mechanical Engineering*, vol. 31, no. 1, pp. 1–16, 2018.

[17] B. Jian and B. C. Vemuri, "Robust point set registration using gaussian mixture models," *IEEE transactions on pattern analysis and machine intelligence*, vol. 33, no. 8, pp. 1633–1645, 2010.

[18] A. Myronenko and X. Song, "Point set registration: Coherent point drift," *IEEE Transactions on Pattern Analysis and Machine Intelligence*, vol. 32, no. 12, pp. 2262–2275, 2010.

[19] R. Horaud, F. Forbes, M. Yguel, G. Dewaele, and J. Zhang, "Rigid and articulated point registration with expectation conditional maximization," *IEEE Transactions on Pattern Analysis and Machine Intelligence*, vol. 33, no. 3, pp. 587–602, 2010.

[20] G. D. Evangelidis and R. Horaud, "Joint alignment of multiple point sets with batch and incremental expectation-maximization," *IEEE transactions on pattern analysis and machine intelligence*, vol. 40, no. 6, pp. 1397–1410, 2017.

[21] N. Ravikumar, A. Gooya, A. F. Frangi, and Z. A. Taylor, "Generalised coherent point drift for group-wise registration of multi-dimensional point sets," in *International Conference on Medical Image Computing and Computer-Assisted Intervention*. Springer, 2017, pp. 309–316.

[22] Z. Min, J. Wang, and M. Q.-H. Meng, "Robust generalized point cloud registration using hybrid mixture model," in *2018 IEEE International Conference on Robotics and Automation (ICRA)*. IEEE, 2018, pp. 4812–4818.

[23] Z. Min, D. Zhu, H. Ren, and M. Q.-H. Meng, "Feature-guided nonrigid 3-d point set registration framework for image-guided liver surgery: From isotropic positional noise to anisotropic positional noise," *IEEE Transactions on Automation Science and Engineering*, 2020.

[24] K. Jordan and P. Mordohai, "A quantitative evaluation of surface normal estimation in point clouds," in *2014 IEEE/RSJ International Conference on Intelligent Robots and Systems*. IEEE, 2014, pp. 4220–4226.

[25] T. Tsujimura and T. Yabuta, "A tactile sensing method for employing force/torque information through insensitive probes," in *Proceedings 1992 IEEE International Conference on Robotics and Automation*, 1992, pp. 1315–1320 vol.2.